

# Mapping the Milky Way with Gaia XP spectra I: Systematic flux corrections and atmospheric parameters for 68 million stars

Xianhao Ye<sup>1,2,3</sup>, Wenbo Wu<sup>1,2,3</sup>, Carlos Allende Prieto<sup>1,2,3</sup>, David S. Aguado<sup>2,3</sup>, Jingkun Zhao<sup>1</sup>, Jonay I. González Hernández<sup>2,3</sup>, Rafael Rebolo<sup>2,3</sup>, Gang Zhao<sup>1,4</sup>, Zhuohan Li<sup>1,4</sup>, Carlos del Burgo<sup>2,3</sup>, Yuqin Chen<sup>1</sup>

<sup>1</sup> CAS Key Laboratory of Optical Astronomy, National Astronomical Observatories, Chinese Academy of Sciences, Beijing 100101, People's Republic of China

<sup>2</sup> Instituto de Astrofísica de Canarias, Vía Láctea, 38205 La Laguna, Tenerife, Spain

<sup>3</sup> Universidad de La Laguna, Departamento de Astrofísica, 38206 La Laguna, Tenerife, Spain

<sup>4</sup> School of Astronomy and Space Science, University of Chinese Academy of Sciences, Beijing 100049, People's Republic of China

Received ? ?, xxxx; accepted ? ?, xxxx

## ABSTRACT

**Context.** Gaia XP spectrophotometry for over two hundred million stars has been publicly released as part of Gaia DR3. These data have great potential for mapping metallicity across the Milky Way. Several recent studies have analyzed this data set to derive atmospheric parameters and identify new metal-poor stars. In addition, systematics in the fluxes of the XP spectra have also been noticed and characterized.

**Aims.** We aim to construct an alternative catalog of atmospheric parameters from Gaia XP spectra by fitting them with synthetic spectra based on model atmospheres, and provide corrections to the XP fluxes according to stellar colors, magnitudes, and extinction.

**Methods.** We use `GaiaXPy` to obtain calibrated spectra and apply `FERRE` to match the corrected XP spectra with models and infer atmospheric parameters. We train a neural network using stars in APOGEE to predict flux corrections as a function of wavelength for each target.

**Results.** Based on the comparison with APOGEE parameters, we conclude that our estimated parameters have systematic errors and uncertainties in  $T_{\text{eff}}$ ,  $\log g$ , and  $[M/H]$  about  $-38 \pm 167$  K,  $0.05 \pm 0.40$  dex, and  $-0.12 \pm 0.19$  dex, respectively, for stars in the range  $4000 \leq T_{\text{eff}} \leq 7000$  K. The corrected XP spectra show better agreement with both models and Hubble Space Telescope CALSPEC data. Our correction increases the precision of the relative spectrophotometry of the XP data from 3.2% – 3.7% to 1.2% – 2.4%. Finally, we have built a catalog of atmospheric parameters for stars within  $4000 \leq T_{\text{eff}} \leq 7000$  K, comprising 68,394,431 sources, along with a subset of 124,188 stars with  $[M/H] \leq -2.5$ . Our catalogs and flux correction code are publicly available from <https://doi.org/10.5281/zenodo.14028589>.

**Conclusions.** Our results confirm that the Gaia XP flux calibrated spectra show systematic patterns as a function of wavelength that are tightly related to colors, magnitudes, and extinction. Our optimization algorithm can give us accurate atmospheric parameters of stars with a clear and direct link to models of stellar atmospheres, and can be used to efficiently search for extremely metal-poor stars.

**Key words.** Techniques: spectroscopic-Catalogs-Stars: fundamental parameters

## 1. Introduction

The stellar metallicities  $[M/H]$  keep track of the formation and evolution of the Milky Way. Due to the chemical enrichment of the interstellar medium by successive stellar generations,  $[M/H]$  can be used as a proxy of age and reflects the birth environment of a star. Assuming that metal-rich disk stars were born on nearly circular orbits in the Galactic plane from chemically well-mixed cold gas, mono-abundance stellar populations with the same metal content ( $[M/H]$ ,  $[\alpha/Fe]$ ) shall be formed at the same birth radius  $R_b$  and look-back time  $\tau$  (Schönrich & Binney 2009). This assumption has been used to establish a comprehensive chemodynamical model of our Galaxy (Sharma et al. 2021; Lian et al. 2022; Imig et al. 2023; Chen et al. 2023; Binney & Vasiliev 2024). Combined with kinematics, the metallicities of metal-poor halo stars serve as a powerful tool to sepa-

rate in-situ populations from the remnants of ancient accretion events (Naidu et al. 2020; Belokurov & Kravtsov 2022; Conroy et al. 2022; Deason & Belokurov 2024). These newly found accreted substructures are useful to check the  $\Lambda$ CDM cosmological paradigm in which Milky Way-sized halos are built from the mergers of smaller satellite galaxies. Extremely metal-poor (EMP) stars may have formed from gas enriched only by the very first stars, also called Pop III (Klessen & Glover 2023). Therefore, their abundance patterns hold the key to constrain nucleosynthesis in the earliest supernova events (Nomoto et al. 2006; Heger & Woosley 2010; Aoki et al. 2014; Nomoto et al. 2013; Koutsouridou et al. 2023). The low-metallicity tail of the metallicity distribution function (MDF) provides essential constraints on the chemical enrichment in the early phases of the formation of the Milky Way (Salvadori et al. 2007; Komiya et al. 2010; Yamada et al. 2013; Sarmiento et al. 2019; Tarumi et al. 2020; Youakim et al. 2020). However, at present only a few hundred stars with  $[M/H] < -3$  and significantly fewer with  $[M/H] < -4$

\* The second author also made substantial contributions to the paper.

\*\* Corresponding author, e-mail: carlos.allende.prieto@iac.es

\*\*\* Corresponding author, e-mail: gzhao@nao.cas.cn

have been identified, and these are insufficient to give a complete picture.

We are witnessing an era in which stellar atmospheric parameters are available for massive samples thanks to large spectroscopic surveys, such as the Sloan Digital Sky Survey (SDSS) I-IV (York et al. 2000; Abazajian et al. 2004; Aihara et al. 2011; Abdurro'uf et al. 2022), the Large Sky Area Multi-Object Fiber Spectroscopic Telescope (LAMOST) survey (Zhao et al. 2006, 2012; Cui et al. 2012; Luo et al. 2012), the Galactic Archaeology with HERMES (GALAH) survey (De Silva et al. 2015; Buder et al. 2021), the SDSS V (Kollmeier et al. 2017), the Dark Energy Spectroscopic Instrument (DESI) survey (Cooper et al. 2023), the 4-metre Multi-Object Spectroscopic Telescope (4MOST) survey (de Jong et al. 2019), or the WHT Enhanced Area Velocity Explorer (WEAVE) survey (Jin et al. 2024). These surveys have already accumulated tens of millions of stellar spectra, and continue to gather more. Combining the spectroscopic data with accurate measurements of proper motions and parallaxes provided by the ESA Gaia mission (Gaia Collaboration et al. 2016, 2023b), enables us to carry out a detailed investigation of the chemodynamic properties of different stellar populations of the Milky Way.

In addition to the astrometric catalog, Gaia Data Release 3 (DR3; Gaia Collaboration et al. 2023b) includes a catalog of 32.2 million high-resolution spectra ( $R \sim 8000$ ) centered on the near infrared Ca II triplet, obtained by the Radial Velocity Spectrometer (RVS) instrument (Cropper et al. 2018; Sartoretti et al. 2018; Andrae et al. 2023a). It also includes a catalog of 220 million low-resolution spectra (hereafter referred to as ‘XP spectra’) obtained with the blue (wavelength range of 330-680 nm) and red (wavelength range of 640-1050 nm) Gaia slitless spectrophotometers, BP and RP, respectively (Carrasco et al. 2021; Montegriffo et al. 2023; De Angeli et al. 2023). The XP spectra have 110 pixels and a variable resolving power, ranging from 20 to 90, as a function of wavelength. The XP spectra in DR3 are represented by Hermite basis functions (Montegriffo et al. 2023).

The Gaia Data Processing and Analysis Consortium (DPAC) has developed the Python library `GaiaXPy`<sup>1</sup> to facilitate handling XP spectra. This software allows the transformation of coefficients into calibrated spectra and photometry. Recent studies have shown that the synthetic photometry from XP spectra can be used to perform a highly precise calibration of other photometry surveys, such as Pristine (Martin et al. 2023), Pan-STARRS (Xiao et al. 2023a), or J-PLUS (Xiao et al. 2023b; Chandra et al. 2023). However, other studies have revealed that XP calibrated spectra suffer from systematic errors that show up as wiggles (Huang et al. 2024), introduced by the combination of noise and the choice of data representation (Weiler et al. 2023). The pattern of wiggles largely depends on the stellar color  $G_{BP} - G_{RP}$  and the apparent magnitude  $G$  (Montegriffo et al. 2023), and may cause a modest bias in the synthetic photometry Huang et al. (2024) and the inferred stellar parameters. Due to its low-resolution and the aforementioned systematics, it is hard to determine chemical abundances from XP spectra. Nonetheless, we are still able to obtain a reliable estimation of the overall metallicity ( $[M/H]$ ) down to the extremely metal-poor domain, as shown using mock XP spectra in Witten et al. (2022). Considering the large data volume and the full sky coverage, XP spectra provide us with a unique opportunity to build a complete metallicity map of the Milky Way.

Previous studies have adopted different methodologies to extract information from the low-resolution XP spectra. Traditional model-driven methods predict the atmospheric parameters by comparing the observed spectra with stellar spectral libraries (e.g., Castelli et al. 1997; Lejeune et al. 1998; Coelho et al. 2005; Gustafsson et al. 2008; Husser et al. 2013; Allende Prieto et al. 2018). As part of the astrophysical parameters inference system (Apsis), the Gaia General Stellar Parameterizer from Photometry (GSP-phot) adopts a Bayesian forward-modelling approach to fit XP spectra with isochrone models and four different stellar libraries (Andrae et al. 2023a). They provided an estimation of effective temperature  $T_{\text{eff}}$ , surface gravity  $\log g$ , metallicity  $[M/H]$ , absolute magnitude  $M_G$ , radius, distance, and extinction for each star. However, the authors of GSP-Phot advised against using these metallicity estimates since they are dominated by large systematic errors.

An et al. (2024) constructed an all-sky 3D extinction map by comparing the low-resolution XP spectra with their empirically-calibrated synthetic spectra, and gave a reliable estimation of metallicity for stars with  $[M/H] > -1$ . Martin et al. (2023) built a model linking the metallicity-sensitive synthetic *CaHK* magnitudes to the photometric metallicity  $[M/H]_{\text{phot}}$  from XP spectra. Even though only  $[M/H]$  measurements are provided, their results show good agreement with the literature in the full metallicity range, even for stars under  $[M/H] = -3$ . Bellazzini et al. (2023) and Xylakis-Dornbusch et al. (2024) also tried to extract metallicity information from the synthetic photometry, but they only determined  $[M/H]_{\text{phot}}$  for a small fraction of the XP spectra available in DR3. The intrinsic nature of the estimation of  $[M/H]_{\text{phot}}$  also involves a comparison between synthetic spectra and observations, albeit indirectly, through the photometry generated from them. The accuracy of model-driven methods highly relies on the consistency between the XP spectra and the synthetic spectra. Unfortunately, there are several points that may induce discrepancies between them.

First, the theoretical spectra are limited by our knowledge of stellar atmospheres, atomic and molecular physics. Second, XP spectra are not perfectly flux-calibrated. Third, the information in the low-resolution spectra is highly sensitive to surface temperature  $T_{\text{eff}}$  and gravity  $\log g$ . The metallicity determined from XP spectra with low ( $T_{\text{eff}} < 4000$  K) and high ( $T_{\text{eff}} > 7000$  K) temperature are likely unreliable, due to the limited strength of metal lines in stars of such low metallicity and high effective temperature.

In the last decade, data-driven and machine learning methods have been widely adopted to overcome the gap between synthetic spectra and observations (e.g., Ness et al. 2015; Ting et al. 2017, 2019; Xiang et al. 2019; Leung & Bovy 2019). Data-driven methods use a large training sample with known labels to construct a relationship between the stellar parameters and the spectra. Previous studies found that data-driven methods are effective to derive precise atmospheric parameters and elemental abundances for low-resolution spectra by applying it to the LAMOST survey (Wilson et al. 2019; Li et al. 2022b; Li & Lin 2023). Therefore, it is natural to turn to data-driven methods to infer stellar properties from XP spectra (e.g., Rix et al. 2022; Andrae et al. 2023b; Zhang et al. 2023; Sanders & Matsunaga 2023; Li et al. 2023; Xylakis-Dornbusch et al. 2024; Laroche & Speagle 2024; Leung & Bovy 2024; Yao et al. 2024; Avdeeva et al. 2024; Fallows & Sanders 2024).

Rix et al. (2022) derived the stellar metallicity for a sample of 2 million giant stars within  $30^\circ$  of the Galactic center using the `XGBoost` algorithm. They achieved a remarkably median precision of  $\delta[M/H] < 0.1$  by adopting the SDSS DR17

<sup>1</sup> <https://gaiaxpy.readthedocs.io/en/latest/cite.html>, DOI v2.1.0: 10.5281/zenodo.8239995

(The Apache Point Observatory Galactic Evolution Experiment, shortened as APOGEE; Abdurro'uf et al. 2022) as the training sample. Andrae et al. (2023b) applied the XGBoost algorithm to the whole catalog and estimated the stellar atmospheric parameters ( $T_{\text{eff}}$ ,  $\log g$ ,  $[M/H]$ ) for over 175 million stars. They have a mean stellar parameter precision of 0.1 dex in  $[M/H]$ , 50 K in  $T_{\text{eff}}$ , and 0.08 dex in  $\log g$ . Besides APOGEE DR17, they also included the metal-poor stars from Li et al. (2022a) in the training sample to break the low-metallicity boundary.

Zhang et al. (2023) developed an empirical forward model using a Neural Network to estimate the stellar atmospheric parameters, distance, and extinction for 220 million stars from XP spectra. Given the stellar parameters, they can provide a prediction of the XP spectra. Laroche & Speagle (2024) developed a novel implementation of a variational auto-encoder which achieves competitive XP spectra reconstructions without relying on stellar labels. Their results suggest that meaningful information related to  $[\alpha/Fe]$  are hidden in the XP spectra. Recently, Li et al. (2023) and Hattori (2024) successfully extracted the information on  $[\alpha/Fe]$  for partial XP spectra by using machine learning models trained on APOGEE DR17. In addition, Leung & Bovy (2024) built a transformer-based model and trained it in a self-supervised manner on a compiled data set. Differently from previous studies, they could not only derive stellar parameters from XP spectra, but also predict the XP spectra giving the stellar labels. In general, data-driven methods are efficient and accurate in analyzing the XP spectra, and have allowed deriving several parameters like  $[\alpha/Fe]$ , that are hard to derive by traditional model-driven methods at such low spectral resolution.

Although data-driven methods have the potential of returning great achievements in exploring the low-resolution XP spectra, their output is highly constrained by the quality of the training data. Most studies adopted APOGEE DR17 as training sample, and several selection criteria are applied to ensure the quality of the stellar labels from APOGEE. Due to those cuts, the  $T_{\text{eff}}$  of the training sample is mainly in the range of 3500 K to 7000 K. Therefore, their constructed models are not applicable to stars outside that temperature range. To cover more spectral types in the training sample, Zhang et al. (2023) combined the standard AFGK catalog from LAMOST DR8 and the hot stars ( $T_{\text{eff}}$ ) catalog from the Hot Payne (Xiang et al. 2022). However, there are systematic differences between these two catalogs, and their model prediction exhibits a large scatter from the literature for stars of  $T_{\text{eff}} > 7500$  K. Besides the limitation in  $T_{\text{eff}}$ , both the APOGEE and LAMOST catalogs have a low boundary of metallicity at  $[M/H] = -2.5$ , which prevents the application of the method to more metal-poor stars. Despite the inclusion of more metal-poor stars from other surveys can remove the low-metallicity boundary, the very small size of the training sample prevents an appropriate coverage of the parameter space, and the metallicity estimations only show a very small improvement at  $[M/H] < -2.5$ . As a comparison, the high-resolution spectroscopic follow-up of metal-poor candidates selected from the catalogs of  $[M/H]_{\text{phot}}$  demonstrated the potential of identifying EMP stars through traditional model-driven methods Xylakis-Dornbusch et al. (2024); Mardini et al. (2024).

In this study, we will combine data-driven and model-driven methods to construct a catalog ( $T_{\text{eff}}$ ,  $\log g$ ,  $[M/H]$ ) for about 68 million stars with XP spectra. To reduce the influence of systematic errors ("wiggles"), we develop a Neural Network (NN) model which corrects the XP spectra according to their stellar labels in Section 4. This correction helps in overcoming the gap between synthetic spectra and observations, and the stellar atmospheric parameters predicted from the corrected spectra are

more reliable, as shown in Section 5. The paper is summarized in Section 6.

## 2. Data

We determine and study systematic errors in the Gaia XP fluxes using a sample of XP spectra cross-matched with the final release of APOGEE, included in the DR17 of the Sloan Digital Sky Survey. We correct the XP spectra using the systematic pattern detected in the APOGEE sample, and check the impact on the inferred stellar atmospheric parameters (comparing to APOGEE) and on the accuracy of the fluxes (comparing to CALSPEC data (Bohlin et al. 2014, 2019; Bohlin & Lockwood 2022)). In this section, we will describe each reference catalog in detail.

### 2.1. Gaia XP spectra

Since XP spectra are described by a set of polynomial coefficients, we use the Python library *GaiaXP* to transform these coefficients into flux-calibrated spectra and synthetic photometry. *GaiaXP* provides an option to represent the spectrum with a smaller set of basis functions, avoiding the noise associated to higher-order terms. In addition to this truncation, we apply a cut in the wavelength range, eliminating regions where the transmission is less than 10%. To remove the influence of the dust extinction, we use the Python package *extinction*<sup>2</sup> adopting the *ccm89* model (Cardelli et al. 1989). The reddening for each individual spectrum is calculated from the two-dimensional SFD dust map (Schlegel et al. 1998; Schlafly & Finkbeiner 2011) using the Python package *dustmap* (Green 2018).

The data analysis code *FERRE* (Allende Prieto et al. 2006)<sup>3</sup>, which matches numerical models to the observations by minimizing the  $\chi^2$ , is used to search for the optimal stellar atmospheric parameters ( $T_{\text{eff}}$ ,  $[M/H]$ , and  $\log g$ ). Several algorithms are available in *FERRE*, and the Powell's UOBYQA algorithm (Powell 2002) is adopted in our work, initializing the search at the grid center. This is a local algorithm, which may lead to incorrect solutions in some cases, but it was chosen due to its high speed, critical for very large samples. We tested applying a Markov chain Monte Carlo algorithm (MCMC, *algor*= 5 in *FERRE*), which performs a global search, to find out that the results are very similar to those obtained with the algorithm adopted in this work. We therefore conclude that Powell's UOBYQA algorithm are both efficient and accurate in this case. We computed a fresh library of model spectra with constant resolution using *Synple*<sup>4</sup>, and Kurucz model atmospheres as in the *nsc* library of Allende Prieto et al. (2018), spanning  $-5 \leq [M/H] \leq +0.5$ ,  $3500 \text{ K} \leq T_{\text{eff}} \leq 8000 \text{ K}$ , and  $1 \leq \log g \leq 5$ . For the model with variable resolution, the upper limit of  $T_{\text{eff}}$  is 12,000 K. This library is publicly released together with this paper.

Gaussian convolution is performed to reduce the resolution of the finely sampled spectral synthesis calculations and match it to the XP data. In this study, we adopt two different resolutions for the model spectra: one is a constant resolution of  $R \sim 104$ , and the other is a variable resolution that changes with the wavelength as the XP spectra (refer to Table 1 in Montegriffo et al. (2023)). For the constant resolution model, the corresponding sampled XP spectrum ( $S_{\text{const}}$ ) ranges from 360 to 990 nm, and has 330 points evenly spaced on a logarithmic scale. For the variable resolution, the corresponding XP spectrum ( $S_{\text{var}}$ )

<sup>2</sup> <https://extinction.readthedocs.io/en/latest/index.html>

<sup>3</sup> <https://github.com/callendeprieto/ferre>

<sup>4</sup> <https://github.com/callendeprieto/synple>

ranges from 360 to 992.1 nm, and has 270 points in increments of the half of Full width at half maximum ( $\text{FWHM} = \frac{\lambda}{R}$ , where  $\lambda$  is the wavelength), based on information from Montegriffo et al. (2023, – see also Carrasco et al. 2021).

FERRE returns the best fitting spectra that most closely resemble the XP observations. The spectra are normalized by their mean values as in Equation 1, and we define the residual  $N\Delta$  Flux as the difference between the normalized fitting ( $N\text{Flux}_{\text{fitting}}$ ) and XP ( $N\text{Flux}_{\text{XP}}$ ) spectra.

$$\begin{aligned} N\text{Flux} &= \text{Flux}/\text{Mean}(\text{Flux}) \\ N\Delta \text{Flux} &= N\text{Flux}_{\text{fitting}} - N\text{Flux}_{\text{XP}} \end{aligned} \quad (1)$$

In previous studies of Montegriffo et al. (2023) and Huang et al. (2024), they also gave a similar definition of the systematic error as  $(\text{Flux}_{\text{XP}} - \text{Flux}_{\text{ref}})/\text{Flux}_{\text{ref}}$  or  $\text{Flux}_{\text{ref}}/\text{Flux}_{\text{XP}}$ , where  $\text{Flux}_{\text{ref}}$  is the corresponding reference spectra from external data. All the fluxes we discuss hereafter are normalized, and the symbol  $N$  will be dropped for clarity. The general shapes of the XP spectra are consistent with the best fitting models in most cases. The residuals are presented in a complex function that oscillates with the wavelength as shown in Figure 1, and its amplitude is usually larger in the blue band than the red band. In this study, we refer to these residuals as "wiggles".

Visual inspection indicates that stars with similar parameters exhibit similar wiggles. To fully understand what are the main parameters that control the pattern, we randomly selected 800,000 stars at different Galactic latitude: 200,000 at low-latitude ( $|b| < 10^\circ$ ), 300,000 at medium-latitude ( $10^\circ \leq |b| < 30^\circ$ ), and 300,000 at high-latitude ( $30^\circ \leq |b| \leq 90^\circ$ ). The corresponding  $\text{Flux}_{\text{fitting}}$  and  $\Delta\text{Flux}$  of these stars are obtained using FERRE. The randomly selected XP sources have an extended distribution in the color-magnitude diagram (CMD), with  $-0.5 < G_{\text{BP}} - G_{\text{RP}} < 3.5$  and  $4 < G < 17.5$ . In section 3 we explore the impact of stellar colors, apparent magnitude, latitude, and metallicity on the wiggles using these randomly selected XP sources.

## 2.2. Metal-poor stars sample

The search for metal-poor stars is one of the most interesting applications of XP data, and therefore we carry out specific evaluations for that type of stars. We selected metal-poor stars from three libraries: JINAbase (Abohalima & Frebel 2018), the Pristine survey (Aguado et al. 2019), and the LAMOST-Subaru metal-poor survey (Li et al. 2022a; Aoki et al. 2022). JINAbase is a collection of chemical abundances and stellar parameters for 1,659 metal-poor stars (60% of which have  $[\text{M}/\text{H}] < -2.5$ ) from the literature, published in the period between 1991 and 2016. The Pristine survey includes a medium-resolution spectroscopic follow-up of 1,007 metal-poor candidates identified from the narrow-band photometry, and more than 900 stars which have been confirmed to have  $[\text{M}/\text{H}] < -2$ . The LAMOST-Subaru survey presented measurements for over 20 elements in 385 stars covering a wide metallicity range from  $-1.7$  to  $-4.3$ . After cross-matching with the XP spectra and applying a cut of  $[\text{M}/\text{H}] < -2$ , our final metal-poor sample consists of 1,813 stars. Most of them are at high-latitude, with  $E(B - V) < 0.1$ . The colors and magnitudes of these stars are roughly in the range of  $0.5 < G_{\text{BP}} - G_{\text{RP}} < 1.5$  and  $6 < G < 17.5$ .

## 2.3. APOGEE DR17

The Apache Point Observatory Galactic Evolution Experiment (APOGEE; Majewski et al. 2017; Wilson et al. 2019) is a large-scale spectroscopic survey of stars in the Milky Way. APOGEE provides high-resolution ( $R = \lambda/\Delta\lambda \sim 22,500$ ) and high signal-to-noise ratio ( $S/N > 70$  typically) spectra throughout the near infrared wavelength range of  $1.51\text{--}1.70 \mu\text{m}$ .

The stellar atmospheric parameters and elemental abundances are determined by the APOGEE Stellar Parameters and Chemical Abundances Pipeline (ASPACP; García Pérez et al. 2016) based on FERRE. APOGEE provides a high-precision study of the kinematics and chemistry of the Milky Way structures (bulge, disk, and halo). The Seventeenth Data Release of the APOGEE survey contains spectra and abundances for 733,901 stars (Abdurro'uf et al. 2022).

## 2.4. CALSPEC Libraries

Considering the wide wavelength coverage of the XP spectra, we chose the CALSPEC library (Bohlin et al. 2014, 2019; Bohlin & Lockwood 2022) as the reference spectra. CALSPEC is a library of flux standards on the HST system. Most of them have a complete STIS (the Hubble Space Telescope's Space Telescope Imaging Spectrograph) coverage of wavelength from the ultraviolet to near-infrared band with a resolving power  $R \approx 560 \sim 700$ . We find 109 CALSPEC stars with XP spectra, and their colors and magnitudes are mainly in the range of  $-1.0 < G_{\text{BP}} - G_{\text{RP}} < 1.5$  and  $4 < G < 18$ . The CALSPEC collection of spectra are likely among the most accurate flux calibrated spectra available, with a 2–3% accuracy in absolute flux. The uncertainty of the monochromatic flux at 555.75 nm (555.6 nm in air) is 0.5% or 0.005 mag (see Bohlin et al. 2014, and the CALSPEC Calibration Database).

## 2.5. LAMOST

LAMOST is a ground-based innovative telescope designed with a large aperture and a wide field-of-view (Zhao et al. 2006, 2012; Cui et al. 2012; Luo et al. 2012). Beginning with a pilot survey in 2011, LAMOST has observed over ten million spectra in the Northern sky with a limiting magnitude of  $r = 17.8$  (Yan et al. 2022).

LAMOST Low-Resolution Spectroscopic (LRS) survey provides low-resolution ( $R \sim 1,800$ ) spectra with a wavelength coverage of  $0.37\text{--}0.90 \mu\text{m}$ . In this study, we use the LRS Stellar Parameter Catalog of A, F, G and K stars from the LAMOST Data Release 11 (DR11), which contains the atmospheric parameters of 7,774,147 stars with a typical error of  $\sim 43$  K for  $T_{\text{eff}}$ , 0.06 dex for  $\log g$ , and 0.04 dex for  $[\text{M}/\text{H}]$ .

## 3. Pattern of wiggles

Comparison between XP spectra and model predicted flux, Montegriffo et al. (2023) shows that the residuals are correlated with  $G_{\text{BP}} - G_{\text{RP}}$  color and  $G$  magnitude. The stellar color is closely associated with surface temperature, which plays a critical role in shaping the spectra energy distribution (SED) through photoionization (Allende Prieto 2023), mainly through hydrogen atoms and the  $\text{H}^-$  ion. The dependence of the wiggles on magnitude may likely be caused by the complex internal calibration of XP spectra. As illustrated by Andrae et al. (2023a), the spectra of stars brighter than  $G = 11.5$  are recorded in 2D windows, which have different read-out configuration (gates) depending on

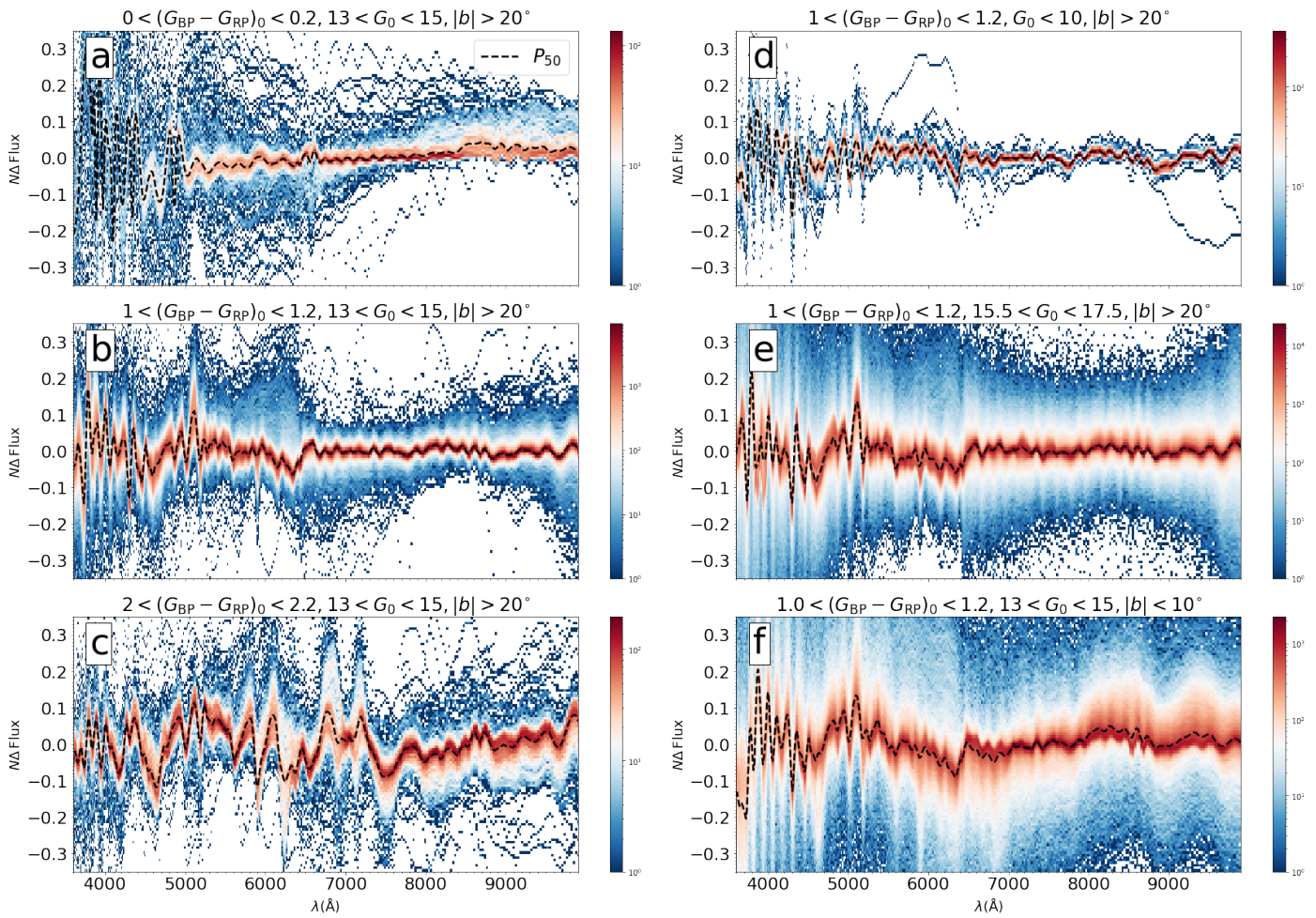


Fig. 1: Density distribution of residuals as a function of wavelength for stars with different parameters. Subfigures a, b, and c are results of stars in bins of the same magnitude range  $13 < G_0 < 15$  but different stellar colors. Subfigures b, d, and e show the density distribution of residuals for stars within the same range of color  $1.0 < (G_{BP} - G_{RP})_0 < 1.2$  but different  $G_0$ . Subfigure f shows the residuals of stars of the same color-magnitude as subfigures b but in different Galactic latitude ( $|b| < 10^\circ$ ). The black dash lines represent the  $P_{50}$  percentiles distributions, which can be viewed as a robust representation of the patterns of wiggles. From the  $P_{50}$  lines we can see that the wiggles change with  $(G_{BP} - G_{RP})_0$  and  $G_0$ , but the stellar color has a larger impact than the magnitude. Stars of low latitudes have a much more diffuse distribution of  $\Delta\text{Flux}$ . The large uncertainties of the extinction map towards the Galactic disc may cause a bad extinction correction of  $\text{Flux}_{XP}$  for some stars. Therefore,  $\text{Flux}_{XP}$  is more likely to deviate from the fitting result  $\text{Flux}_{fitting}$  for stars of lower latitudes.

magnitude, while fainter stars are mainly observed as 1D windows and under a more uniform readout strategy. Montegriffo et al. (2023) noted that a built-in assumption in the external-calibration (calibrating the internally-calibrated continuously-represented mean spectra to an absolute system) is that the instrument model is independent of brightness (or magnitude). Therefore, it cannot easily account for inconsistencies caused by the different observing modes, which may finally result in a correlation between residuals and  $G$  magnitude.

Inspired by previous studies, we randomly distribute our selected XP sources, limited to  $E(B - V) < 2$ , into different bins in de-reddened  $(G_{BP} - G_{RP})_0$  color and  $G_0$  magnitude. Figure 1 shows the density distribution of residuals as a function of wavelength for stars with different values of  $(G_{BP} - G_{RP})_0$ ,  $G_0$ , and Galactic latitude  $b$ . We find that the wiggles change dramatically with color. For stars in the same color bins, we can see some scatter, but most of them have a very similar pattern, especially for stars in the range  $1.0 < (G_{BP} - G_{RP})_0 < 1.2$ .

Panels (b), (d), and (e) of Figure 1 show the distributions of residuals for stars with the same color but different magnitude  $G_0$ . The residuals' pattern clearly changes with  $G_0$  as well, although to a lesser extent than with  $(G_{BP} - G_{RP})_0$ . The stellar color is a major determining factor of the SED, while the apparent magnitude  $G_0$  is connected to the SED through the instrument model. Since the wiggles in the residuals largely depend on the SED, it is only natural that the stellar color plays a much more important role. For stars in the same color-magnitude bin but located at lower Galactic latitudes, the general pattern is similar, but the residuals have a much more diffuse distribution. We conclude that the stellar color  $G_{BP} - G_{RP}$ , apparent magnitude  $G$ , and dust extinction  $E(B - V)$  should be considered when modeling the observed systematic patterns.

Huang et al. (2024) also considered the intrinsic color and extinction in their proposed corrections, but disregarded the weaker effects of  $[M/H]$  and  $\log g$ . This choice simplifies the correcting process, focusing on the accuracy of the correction for most stars. However, the libraries they used mainly consist

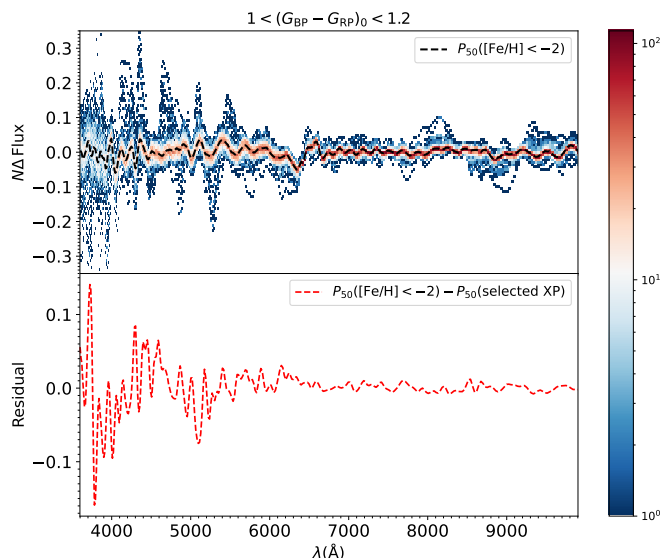


Fig. 2: Top panel shows the density distribution of the residuals of very metal-poor stars with  $1.0 < G_{BP} - G_{RP} < 1.2$  and  $13 < G < 15$ . Compared to the relatively more metal-rich sample in Figure 1, their wiggles have a smaller amplitude with  $\text{Max}(|P_{50}|) < 0.08$ . The bottom panel shows the difference of  $P_{50}$  between these two samples. The main difference is in the blue band of  $\lambda < 6500\text{\AA}$ , while the wiggles in the red band is little affected by the change of metallicity.

of stars with  $[M/H] > -1$ , and the SEDs of very metal-poor stars are quite different from those of metal-rich ones. To fully understand the influence of  $[M/H]$ , we adopt the sample from subsection 2.2, and obtain its density distribution of residuals in Figure 2. We can see that the largest differences concentrate on the blue band, where the residuals of very metal-poor stars have a smaller amplitude with the maximum absolute value  $\text{Max}(|P_{50}|) < 0.08$ . In general, the pattern of fitting residuals for very metal-poor stars is far more featureless than for metal-rich stars. Since one of our aims is to make an accurate estimation of metallicity from the wiggle-corrected XP spectra, we should take extra care with the influence of  $[M/H]$ .

## 4. Method

Our aim is to correct the wiggles observed in the residuals for a given spectrum and calculate atmospheric parameters by fitting the observations with model spectra using FERRE. Therefore, we first need to characterize the systematic patterns as a function of color, magnitude, reddening and metallicity. This is what machine learning is good at. Therefore, we use the main relevant parameters as input into a neural-network model with multiple hidden layers, where the residuals from the fits are the output. We may not have the information of metallicity for a given star. Therefore, we strongly prefer to avoid using metallicity as input, and instead adopt various metallicity-sensitive photometric indices.

It is important to stress that there is a limited number of spectra with metallicity below  $-2.5$  to train the NN model, so we do not trust and do not apply the derived correction to stars with metallicity under  $-2.5$ . In this section, we describe first how we predict the correcting patterns via the NN, including the training dataset and the architecture of our NN model. Then we provide

additional details on how we correct and fit all XP spectra in DR3.

### 4.1. Training Database

To ensure the patterns in the residuals we characterize really reflect the differences between the XP and the theoretical spectra, we only use spectra with reliable estimations of atmospheric parameters, judging from the differences with the APOGEE parameters. We refer to the resulting sample as the training APOGEE sample (TAS) hereafter. The APOGEE sample is firstly cleaned by applying the cuts below, where the symbol A indicates APOGEE parameters:

- $S/N > 70$ ;
- $\sigma_{T_{\text{eff}}^A} \leq 250$ ,  $\sigma_{\log g^A} \leq 0.5$ ;
- $3500 \leq T_{\text{eff}}^A \leq 8000$  K or  $\leq 12000$  K,  $1 \leq \log g^A \leq 5$ .

We tested two different values as the upper limits of  $T_{\text{eff}}^A$  for the two different models for the resolution of XP spectra. The upper limit is 8000 K for  $S_{\text{const}}$ , and 12000 K for  $S_{\text{var}}$ . In the APOGEE DR17 catalog, there are some sources with Gaia source\_id = 0, which are dropped in our APOGEE sample. In addition, for sources with the same Gaia source\_id, we only keep the first one ( $\sim 10\%$  sources are duplicated). Then we obtain the initial parameters for the APOGEE sample (IAS). Next, we calculate the atmospheric parameters for XP spectra using FERRE. After deriving  $T_{\text{eff}}$ ,  $\log g$ , and  $[M/H]$ , we trim down the IAS applying the following constraints:

- $|T_{\text{eff}}^{\text{XP}} - T_{\text{eff}}^A| < 200$
- $|\log g^{\text{XP}} - \log g^A| < 0.5$
- $|[M/H]^{\text{XP}} - [M/H]^A| < 0.5$ ,

where  $T_{\text{eff}}^{\text{XP}}$ ,  $\log g^{\text{XP}}$ ,  $[M/H]^{\text{XP}}$  are parameters estimated from the Gaia XP spectra by FERRE. Finally, our TAS includes 157,478 stars for  $S_{\text{const}}$ , and 131,173 stars for  $S_{\text{var}}$ .

### 4.2. Input and Output

As we mentioned before, the shape of the residuals are highly related to the color, magnitude, and reddening of a star and, to a lesser extent, to its metallicity. Therefore, we use various of colors and magnitudes, including metallicity-sensitive colors, generated from XP spectra, as input for our NN model. We employ GaiaXPpy and the built-in photometric system (Gaia Collaboration et al. 2023a) to obtain the SkyMapper magnitudes  $u$ ,  $v$ ,  $g$ ,  $i$ , and the metallicity-sensitive colors (Chiti et al. 2021)  $g - i$ ,  $v - g - 0.9 \times (g - i)$ , and  $u - v - 0.9 \times (g - i)$ . In addition, the reddening  $E(B - V)$  calculated from dustmaps is included as one of the parameters.

To summarize, the 14 parameters involved are:

- metallicity-sensitive colors:  $g - i$ ,  $v - g - 0.9 \times (g - i)$ ,  $u - v - 0.9 \times (g - i)$
- SkyMapper photometric passbands:  $u$ ,  $v$ ,  $g$ ,  $i$
- Gaia photometric passbands and colors: `phot_g_mean_mag`, `phot_bp_mean_mag`, `phot_rp_mean_mag`, `bp_rp`, `bp_g`, `rp_g`
- reddening:  $E(B - V)$ .

The output is the predicted flux corrections as a function of wavelength.



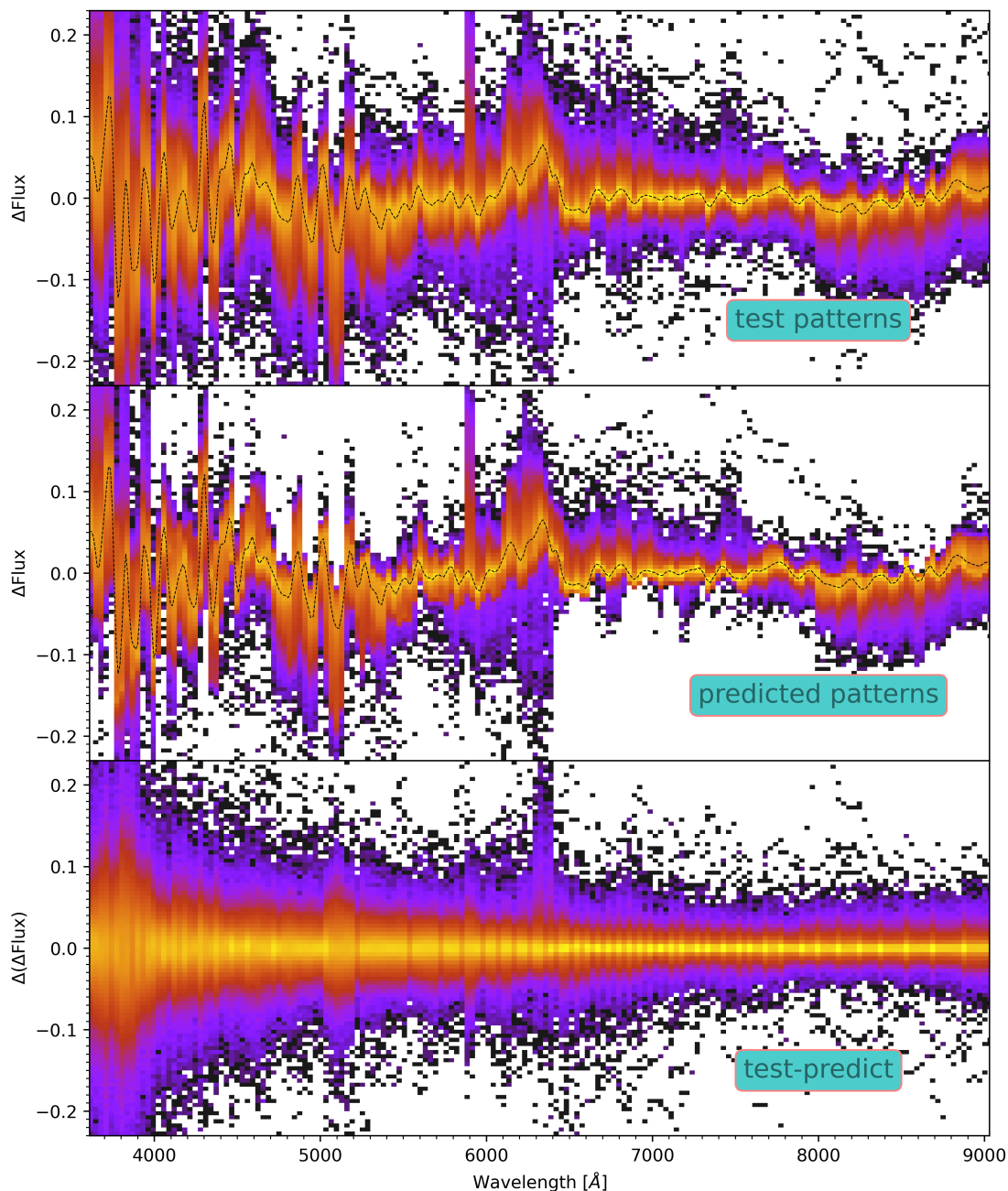


Fig. 4: Comparison between the real patterns from TAS (20% of the whole sample, top panel) and the NN model predicted patterns (middle panel). The bottom panel shows the difference between the real and predicted patterns, from which we can see that the wiggles disappear.

XP spectra is 330 nm, covering most wavelength range of the  $u$  band and the full wavelength range of the  $v$  band. However, `GaiaXPy` fails to generate these two bands for some spectra, primarily for faint stars, though not all faint stars are affected by this issue.

## 5. Results

In this section, we discuss the estimation of parameters for the IAS after correcting the systematic pattern predicted by our NN model trained on the TAS data set. As described below, this correction makes the XP spectra fit the model spectra better, and in

particular, we find a significantly better agreement with the HST CALSPEC observations.

### 5.1. Stellar atmospheric parameters

Besides determining the absolute flux, we find that the correction of the systematic pattern can improve the estimation of stellar atmospheric parameters from XP spectra. We first calculate parameters from XP spectra with sampling  $S_{\text{const}}$ . In Figure 5 we show the distributions of the stellar atmospheric parameters ( $T_{\text{eff}}$ ,  $\log g$ ,  $[M/H]$ ) inferred from the original and wobble-corrected spectra, comparing with parameters from the APOGEE survey. The top and middle panels compare parameters from XP and



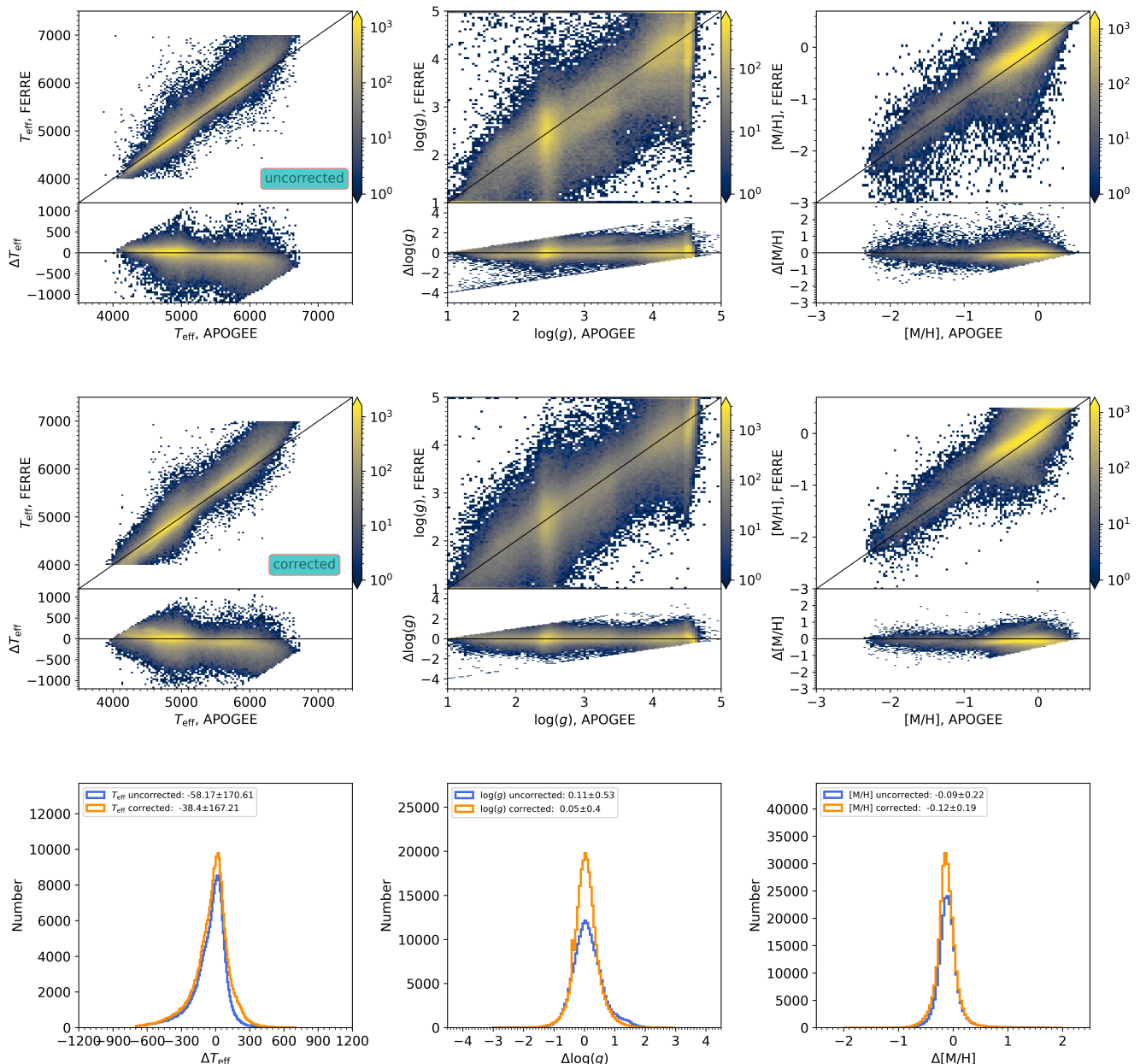


Fig. 5: Testing on atmospheric parameters using sampling  $S_{\text{const}}$ . Top panels: Comparison of  $T_{\text{eff}}$ ,  $\log g$  and  $[M/H]$  estimated from original XP spectra (Y-axis) and APOGEE survey (X-axis). Middle panels: Similar to the top panels, but with Y-axis replaced by the results from corrected XP spectra. The color bar in each subfigure displays the number density. Bottom panels: Histograms present the differences of  $T_{\text{eff}}$ ,  $\log g$  and  $[M/H]$  between XP and APOGEE before and after correcting the systematic patterns. The mean values and standard deviations are shown in the labels.

APOGEE before and after the correction. We keep stars with  $4000 \leq T_{\text{eff}} \leq 7000$  K to compare with APOGEE, because our analysis for stars with lower and higher temperatures performs worse. In addition, the stars in this figure have passed the selection based on the quality flag `dflux_per`, which describes the percentage of data points from  $\Delta \text{Flux} \equiv \text{Flux}_{\text{XP}} - \text{Flux}_{\text{model}}$  exceeding 0.05. We retain stars with `dflux_per` below 20% before the correction and 8% after the correction. It is worth noting that more stars remain after correction, as the correction improves the fit between the XP spectra and the models. As a result, even with more stringent selection criteria, we still obtain more stars than before the correction.

Figure 5 shows that our estimations are highly consistent with APOGEE’s parameters both before and after corrections within the range  $4000 \leq T_{\text{eff}} \leq 7000$  K. But comparing the middle panels with the top panels, one can easily find that estimations for  $T_{\text{eff}}$ ,  $\log g$  and  $[M/H]$  become somewhat better after correction, especially when examining the differences in  $\log g$  and  $[M/H]$ . Correcting the systematic pattern not only reduces the biases in  $T_{\text{eff}}$  and  $\log g$ , but it also makes our results more precise, as suggested from the smaller dispersion relative to APOGEE results.

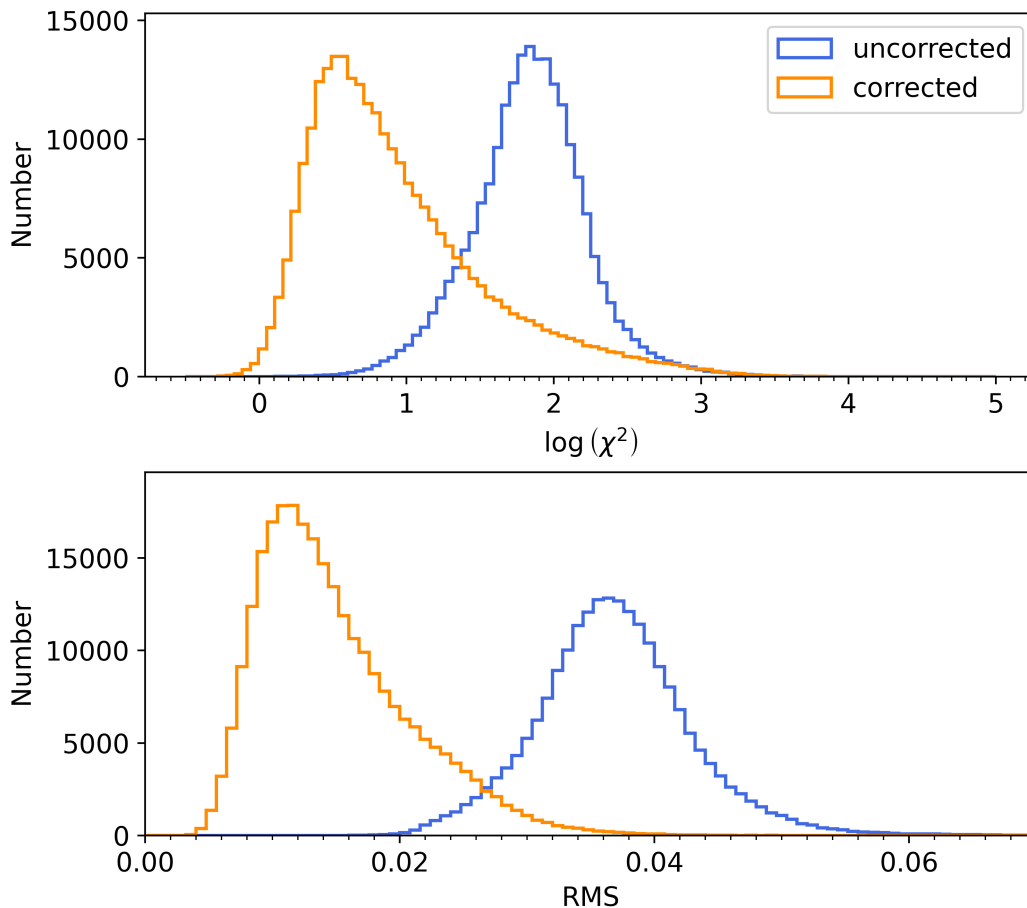


Fig. 6: Histograms present  $\log(\chi^2)$  and RMS between the XP spectra and model spectra for the IAS data set before and after correcting the pattern, indicating by blue and orange, respectively.

We provide below a brief summary of the changes in the mean value and standard deviation of  $\Delta T_{\text{eff}}$ ,  $\Delta \log g$ , and  $\Delta[\text{M}/\text{H}]$  for the nominal  $S_{\text{const}}$  analysis:

- $\Delta T_{\text{eff}}$ : from  $-58.17 \pm 170.61$  to  $-38.40 \pm 167.21$ ;
- $\Delta \log g$ : from  $0.11 \pm 0.53$  to  $0.05 \pm 0.40$ ;
- $\Delta[\text{M}/\text{H}]$ : from  $-0.09 \pm 0.22$  to  $-0.12 \pm 0.19$ .

The most significant improvement is in the estimation of  $\log g$ , where the dispersion  $\sigma_{\Delta \log g}$  is reduced from 0.53 to 0.40.

We also calculate parameters for  $S_{\text{var}}$  for the same sample of stars (IAS) with the same selection rules. We find that  $\Delta T_{\text{eff}}$ ,  $\Delta \log g$ , and  $\Delta[\text{M}/\text{H}]$  are very similar with previous results using sampling  $S_{\text{const}}$ , summarized as follows.

- $\Delta T_{\text{eff}}$ : from  $-62.11 \pm 177.21$  to  $-50.28 \pm 163.46$ ;
- $\Delta \log g$ : from  $-0.09 \pm 0.73$  to  $-0.05 \pm 0.47$ ;
- $\Delta[\text{M}/\text{H}]$ : from  $-0.13 \pm 0.23$  to  $-0.14 \pm 0.19$ .

Despite the overall results are quite similar for the two different samplings, those for  $S_{\text{const}}$  before correcting patterns are slightly better. After correcting the patterns, we find that  $\Delta T_{\text{eff}}$ ,  $\Delta \log g$ , and  $\Delta[\text{M}/\text{H}]$  from the two samplings are similar. However, the constant sampling still seems to provide better results, especially for  $T_{\text{eff}}$  and  $\log g$ . Therefore, we adopt constant sampling in the following sections and our series of papers.

## 5.2. Flux corrections

Correcting the wiggles has a significant impact on the fitting of XP spectra. We examine the  $\log(\chi^2)$  and RMS distributions and both parameters are significantly reduced, as shown in Figure 6 for the stars in the IAS. The RMS is defined:

$$\text{RMS} = \sqrt{\frac{1}{n} \sum_i (F_i^{\text{XP}} - F_i^{\text{model}})^2} \quad (2)$$

where  $F^{\text{XP}}$ ,  $F^{\text{model}}$  are the fluxes of XP spectrum and model spectrum,  $i$  indicates the points of sampling, and  $n$  is the number of data points. Our correction makes  $\log(\chi^2)$  and RMS becoming way much smaller. As shown in the bottom panel of Figure 6, the peak of the RMS histogram decreases from 3.7% to 1.2%. In the following we check whether the correction helps in bringing the XP spectra closer to the CALSPEC data, which have a superb flux calibration.

## 5.3. The CALSPEC library

Given the excellent absolute flux calibration of the CALSPEC spectra, we use this library to perform an independent check of our proposed corrections. Since they have significantly larger resolving power, we apply Gaussian convolution to match their resolution to the XP spectra (and our model spectra). Then, we

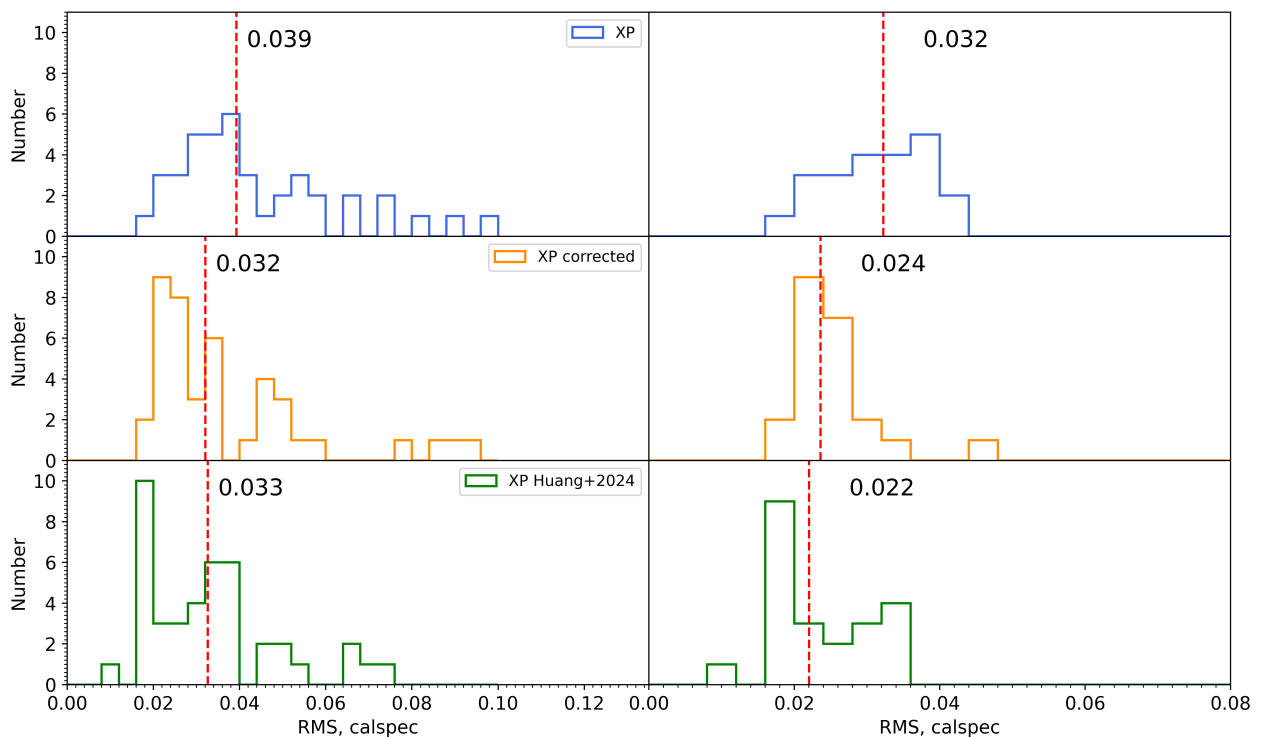


Fig. 7: Left panels: Histograms present RMS between the XP spectra and the spectra from CALSPEC libraries before and after correcting patterns, indicating by blue and orange, respectively. The green histogram shows the corresponding results obtained using the Python package from Huang et al. (2024) to correct the XP spectra. Right panels: Similar to those panels in the left, but with stars passed the quality cuts applied in the Section 5.1. The red dashed lines represent the median values, which are also indicated by the number displayed in each panel.

perform an interpolation of the smoothed spectra to match the sampling of XP data, and correct extinction in the same way we do for the XP spectra. Only spectra of stars estimated to have  $T_{\text{eff}} < 10^4$  K are used in this comparison, based on the parameter `teff_gsphot` in Gaia DR3.

We firstly checked the RMS between the XP spectra and the spectra from CALSPEC, comparing the results before and after the correction. All spectra from XP and CALSPEC are de-reddened with the same method (see in Section 2). The results for stars without quality cuts are shown in the left-hand panels of Figure 7, and the right panels display the results for stars that passed the quality cuts. We find that the RMS with the correction of the pattern is overall reduced, with only one exception for stars that passed the quality cuts. From the median RMS values, indicated by the red dashed lines in the figure, our correction reduces the RMS from 3.9% to 3.2%, or from 3.2% to 2.4%, depending on whether quality cuts are applied. Overall, the XP spectra are fit better with CALSPEC after correcting the systematic pattern. We also use the package provided by Huang et al. (2024) to correct XP spectra as a comparison, shown in the two subfigures in the bottom panels. We de-redden and interpolate the spectra corrected by the package to match the sampling used in this paper, because the default sampling in our work differs from that of Huang et al. (2024). From the orange and green histograms, shown in the middle and bottom panels in Figure 7, the overall improvements from our correction and the correction by Huang et al. (2024) are comparable, regardless of whether quality cuts are applied. We should also mention that the resolution of our model spectrum is not exactly the same as that of the XP spectrum, as we use a constant resolution of around 100. There-

fore, the comparison is not perfect. However, we have checked the results using variable resolution and reach the same conclusions.

We also present plots for a few individual XP spectra comparing them to CALSPEC in Figure 8. After correcting the pattern, the XP spectra match better the CALSPEC data smoothed to the resolution of the Gaia spectrophotometry. Nonetheless, there are some wavelengths at which the corrected version gives poorer agreement with CALSPEC. We have also repeated the check with the Next Generation Spectral Library (NGSL; Gregg et al. 2006; Pal et al. 2023), but the improvement is not so clear, which we associate to the lower quality of the flux calibration of the library compared to the exquisite CALSPEC data.

#### 5.4. Atmospheric parameters catalog of Gaia XP spectra

In Section 4.4 we describe our analysis of the whole sample of Gaia XP spectra. Using the same restrictions in Section 5.1 ( $4000 \leq T_{\text{eff}} \leq 7000$  K, and a maximum of 8% of the data points with  $\Delta\text{Flux}$  larger than 0.05), we build our catalogs of stellar parameters for stars with Gaia XP spectra. We have a global catalog containing 68,394,431 stars, and a metal-poor catalog containing 124,188 stars that have  $[M/H] < -2.5$  and  $A_V \leq 1.5$ . The global catalog has also been cross-matched with LAMOST DR11 low-resolution catalog using the Gaia `source_id`, finding 3,006,606 common sources. We compare the atmospheric parameters  $T_{\text{eff}}$ ,  $\log g$ , and  $[M/H]$  between our results and LAMOST in Figure 9.

We also compare our results with recent catalogs from literature. Since machine learning results can exhibit artificially

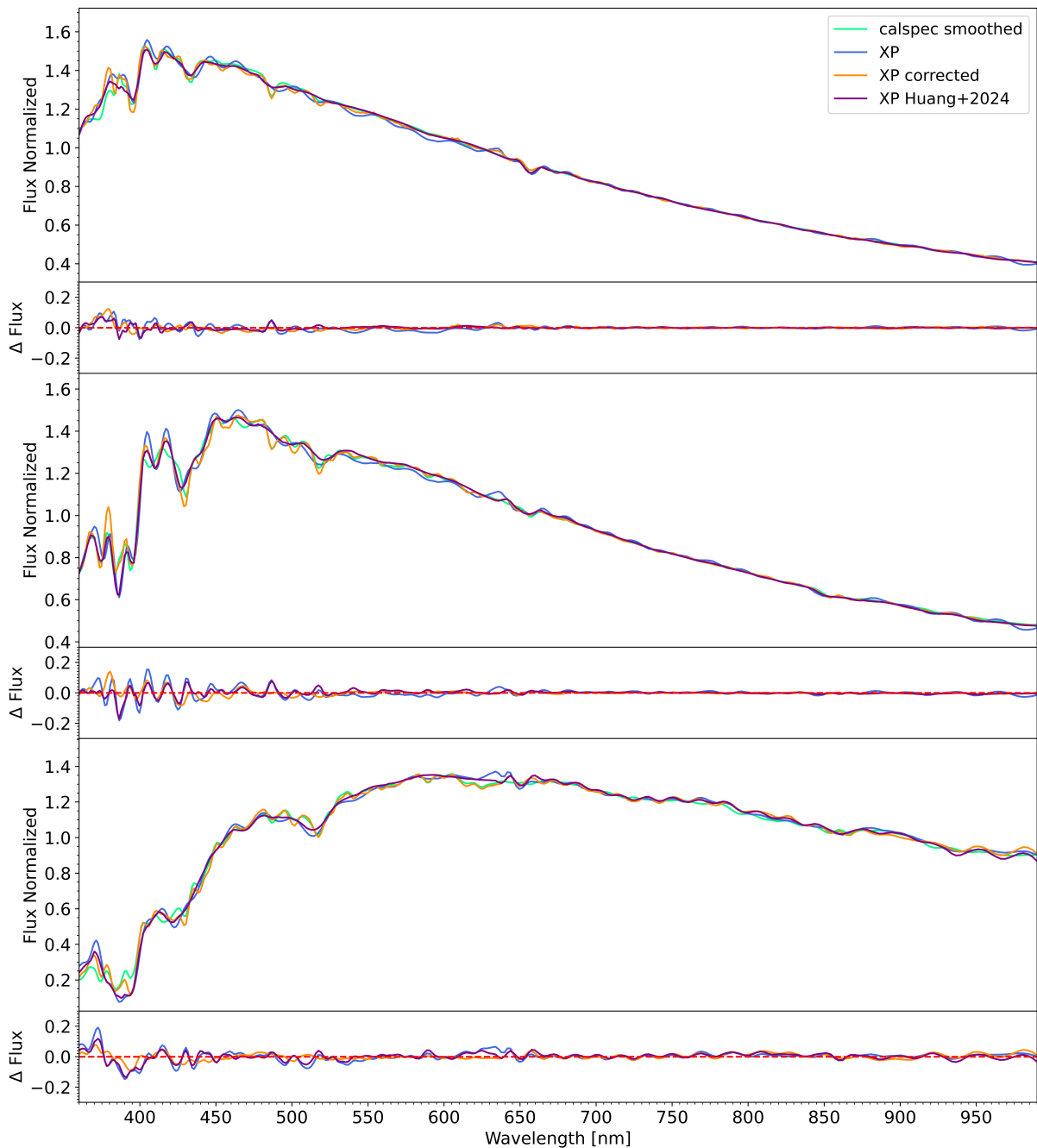


Fig. 8: Examples of how pattern correction can help improve the fitting between the XP spectra and the CALSPEC. Three spectra with different temperature are presented in the sub-panels. In each panel, the XP spectra with and without correcting patterns, smoothed CALSPEC spectra are shown with different colors. The purple lines show the corrected spectra using the package provided by Huang et al. (2024). The  $\Delta\text{Flux}$  between XP and CALSPEC are also presented in each panel.

high performance on the training data, as the data is used to optimize model parameters, we will use parameters from different surveys as reference points in our comparison. Andrae et al. (2023b) provides atmospheric parameters using XGBoost training on APOGEE. To make a fair comparison, we cross-match

our catalog and theirs with LAMOST DR11 low-resolution catalog. With no additional cuts, there are almost 3 million stars in common. We calculate  $\Delta T_{\text{eff}}$ ,  $\Delta \log g$ ,  $\Delta [M/H]$  between our results and the results from LAMOST, which are presented in the three top panels in Figure 10.  $\Delta T_{\text{eff}}$ ,  $\Delta \log g$ ,  $\Delta [M/H]$  between

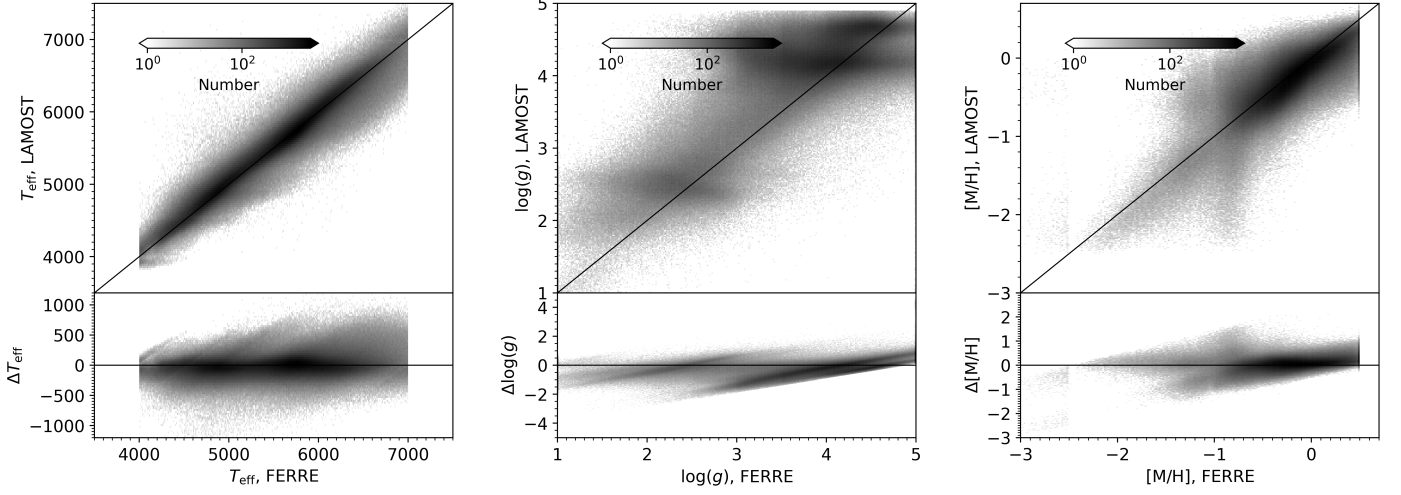


Fig. 9: Compare atmospheric parameters  $T_{\text{eff}}$ ,  $\log g$ , and  $[M/H]$  between our catalog and LAMOST DR11 low-resolution catalog.

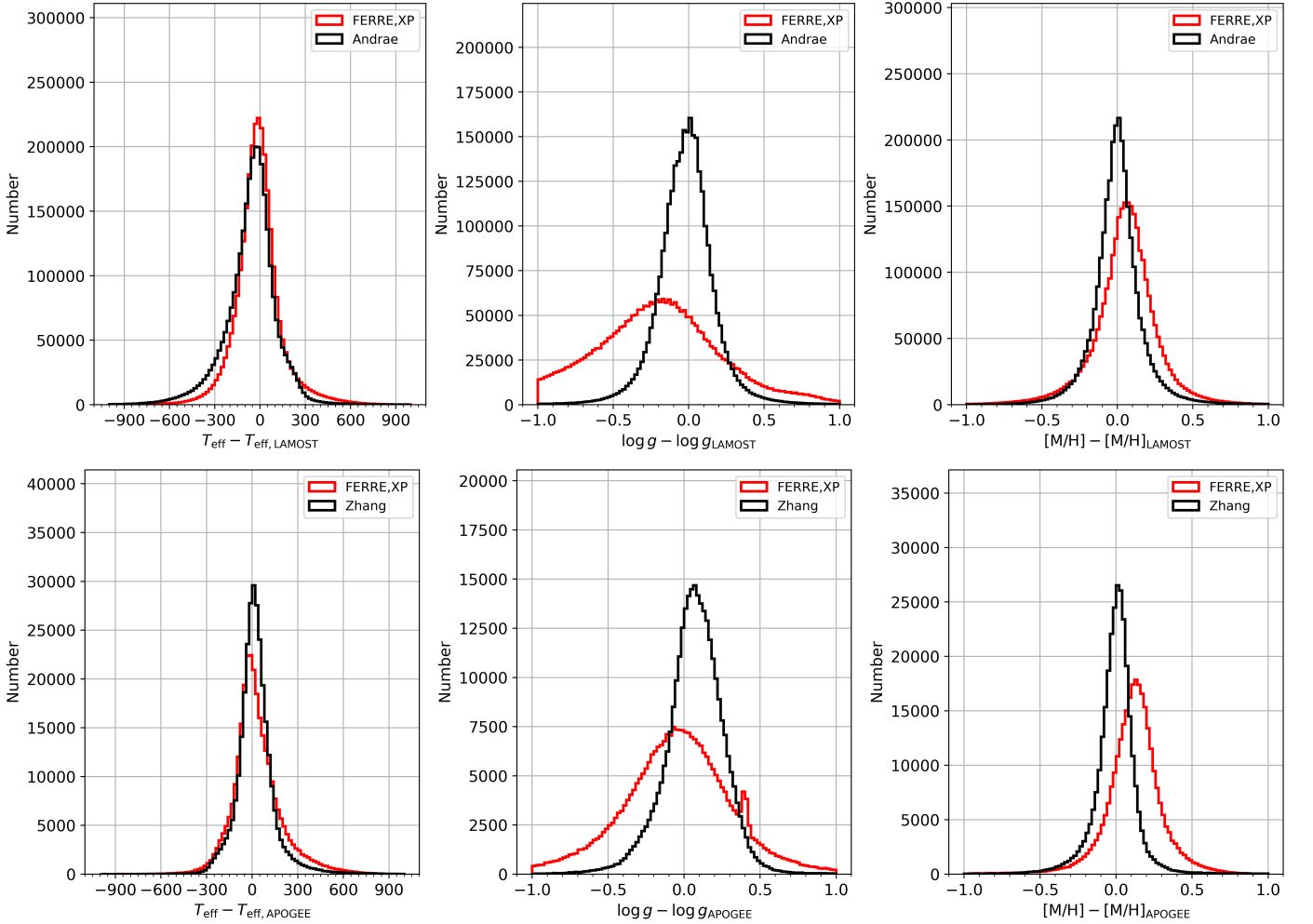


Fig. 10: Comparison of our catalog with other catalogs from literatures using LAMOST or APOGEE as references. Top panels: Histograms in red showing the differences in atmospheric parameters between our catalog and the catalog from LAMOST. Histograms in black showing the differences between the catalog from Andrae et al. (2023b) and the one from LAMOST. Bottom panels: Similar to the top panels, we compare our catalog with the catalog from Zhang et al. (2023) using APOGEE as a reference.

Andrae et al. (2023b) and LAMOST are also presented in those panels with different colors. We can see that we have a better

estimation for  $T_{\text{eff}}$  when using the reference  $T_{\text{eff}}$  from LAMOST. However, our gravity estimation is significantly worse than

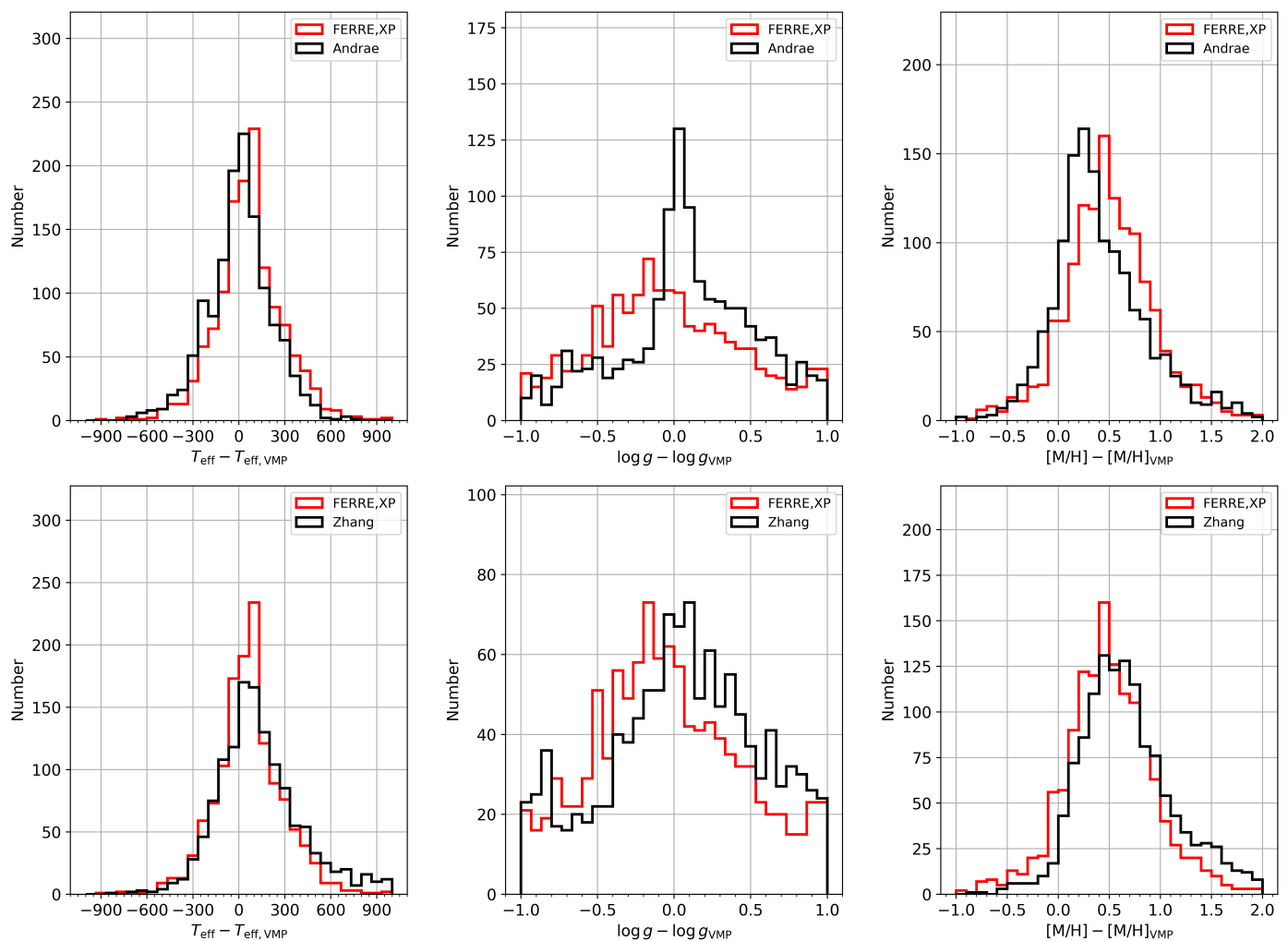


Fig. 11: Similar to Figure 10, Comparison of our catalog with other catalogs from literatures using VMP stars as references.

theirs, and the metallicity from Andrae et al. (2023b) is also better than ours. In the three bottom panels, we compare our results with Zhang et al. (2023). We use APOGEE DR17 as a reference to calculate  $\Delta T_{\text{eff}}$ ,  $\Delta \log g$ ,  $\Delta [M/H]$  between our catalog (or the catalog from Zhang et al. (2023)) with the catalog from APOGEE. From these histograms, using APOGEE as a reference, all three atmospheric parameters from Zhang et al. (2023) are better than ours.

Both of the analysis by Andrae et al. (2023b) and Zhang et al. (2023) are different in nature from us. Not only they employ data-driven method, while our results are obtained from synthetic spectra based on model atmospheres, but they make use of the trigonometric parallaxes from Gaia, while we do not. We plan to adapt our algorithm to make use of that valuable information, which can directly and dramatically improve the retrieved surface gravities, as well as constraining better the effective temperatures and metallicities.

In addition, the most used training datasets for machine learning, such as the catalogs from APOGEE and LAMOST, have a fairly restrictive lower boundary in metallicity, which limits their application to detect metal-poor star candidates. We cross-matched our catalog with VMP stars and the catalogs from the literature described in §2.2. It should be pointed out that Andrae et al. (2023b) used metal-poor stars to replenish their training sample, which contains many sources in common with our

VMP selection. Therefore, comparison between our results and their for VMP stars is not fair. Not surprisingly, Andrae et al. (2023b) performs better in such comparison, but our method performs better compared to Zhang et al. (2023), as shown in Figure 11. In conclusion, our catalog offers some advantages in the parameter range beyond those covered by previous work, and has more clean and direct connection to physical models of stellar atmosphere.

The first column in our global catalog is name, representing the Gaia source\_id of each source. Following this, we provide the atmospheric parameters and their corresponding errors:  $T_{\text{eff}}$ ,  $\log g$ ,  $\text{FeH}$ ,  $T_{\text{eff\_err}}$ ,  $\log g_{\text{err}}$ , and  $\text{Feh\_err}$ . The  $\chi^2$  value for each spectrum is also included in the column `chi2`. Another parameter reflecting the quality of the atmospheres parameters in our catalog is `dflux_per`, as discussed earlier in Section 5.1. This quality flag has already been used to select reliable results, and one can apply stricter criteria, such as `dflux_per < 0.10` or `0.12`, to identify even more reliable sources. For the metal-poor catalog, we also include the extinction  $A_V$  used in this paper. Additionally, the catalog is cross-matched with Gaia to obtain various parameters from Gaia DR3, such as proper motion and magnitude. The global and metal-poor catalogs, along with the code for correcting the systematic patterns in the spectra, are made publicly available.

## 6. Summary

In this paper, we characterize the patterns of systematic errors present in the absolute-calibrated Gaia XP spectra, using a very large number of XP spectra and their best-fitting synthetic spectra based on model atmospheres. We find that those patterns depend on stellar colors, brightness, extinction, and metallicity. We present a simple Neural Network (NN) that relates the systematic flux patterns with stellar color, magnitude, and extinction. The predicted patterns match those in the data very well. After correcting the wiggles, FERRE is applied to derive atmospheric parameters from corrected Gaia XP spectra. Our methodology is validated from the comparison with APOGEE DR17 parameters and stars with observations in the HST CALSPEC collection.

Compared to APOGEE, our estimation of atmospheric parameters is accurate in the temperature range  $4000 \leq T_{\text{eff}} \leq 7000$  K, with slight systematic errors and standard deviations around  $-38 \pm 167$  K,  $0.05 \pm 0.40$  dex, and  $-0.12 \pm 0.19$  dex in  $T_{\text{eff}}$ ,  $\log g$ , and  $[M/H]$ , respectively. The estimation of atmospheric parameters and spectra flux are both improved by correcting the systematic patterns. Our corrections improve the quality of the relative spectrophotometry of the Gaia XP data from 3.2% – 3.7% to 1.2% – 2.4%, as verified against our models and the high-quality CALSPEC standards. Finally, we publish our atmospheric parameters catalog of 68,394,431 sources, with a metal-poor ( $[M/H] \leq -2.5$ ) subset including 124,188 stars, and our results are compared with alternative catalogs published recently. Our catalogs and flux-correction code are publicly available.

*Acknowledgements.* This study is supported by the National Natural Science Foundation of China under grant Nos. 11988101, 12273055, 11927804, and the National Key R&D Program of China, under grant Nos. 2019YFA0405500, 2023YFE0107800. This study is also supported by International Partnership Program of Chinese Academy of Sciences. Grant No. 178GJHZ2022040GC. Xianhao Ye and Wenbo Wu acknowledge the support from the China Scholarship Council. CAP acknowledges financial support from the Spanish Ministry MICIU projects AYA2017-86389-P and PID2020-117493GB-I00. This research made use of computing time available on the high-performance computing systems at the Instituto de Astrofísica de Canarias. The authors are thankful for the technical expertise and assistance provided by the Spanish Supercomputing Network (Red Española de Supercomputación), and the staff at the Instituto de Astrofísica de Canarias. This work presents results from the European Space Agency (ESA) space mission Gaia. Gaia data are being processed by the Gaia Data Processing and Analysis Consortium (DPAC). Funding for the DPAC is provided by national institutions, in particular the institutions participating in the Gaia MultiLateral Agreement (MLA). The Gaia mission website is <https://www.cosmos.esa.int/gaia>. The Gaia archive website is <https://archives.esac.esa.int/gaia>. This job has made use of the Python package GaiaXPpy, developed and maintained by members of the Gaia Data Processing and Analysis Consortium (DPAC), and in particular, Coordination Unit 5 (CU5), and the Data Processing Centre located at the Institute of Astronomy, Cambridge, UK (DPCI). Funding for the Sloan Digital Sky Survey IV has been provided by the Alfred P. Sloan Foundation, the U.S. Department of Energy Office of Science, and the Participating Institutions. SDSS-IV acknowledges support and resources from the Center for High Performance Computing at the University of Utah. The SDSS website is [www.sdss4.org](http://www.sdss4.org). SDSS-IV is managed by the Astrophysical Research Consortium for the Participating Institutions of the SDSS Collaboration including the Brazilian Participation Group, the Carnegie Institution for Science, Carnegie Mellon University, Center for Astrophysics | Harvard & Smithsonian, the Chilean Participation Group, the French Participation Group, Instituto de Astrofísica de Canarias, The Johns Hopkins University, Kavli Institute for the Physics and Mathematics of the Universe (IPMU) / University of Tokyo, the Korean Participation Group, Lawrence Berkeley National Laboratory, Leibniz Institut für Astrophysik Potsdam (AIP), Max-Planck-Institut für Astronomie (MPIA Heidelberg), Max-Planck-Institut für Astrophysik (MPA Garching), Max-Planck-Institut für Extraterrestrische Physik (MPE), National Astronomical Observatories of China, New Mexico State University, New York University, University of Notre Dame, Observatorio Nacional / MCTI, The Ohio State University, Pennsylvania State University, Shanghai Astronomical Observatory, United Kingdom Participation Group, Universidad Nacional Autónoma de México, University of Arizona, University of Colorado Boulder, University of Oxford, University of Portsmouth, University of Utah, University of Virginia,

University of Washington, University of Wisconsin, Vanderbilt University, and Yale University. This work made extensive use of TOPCAT (Taylor 2005).

## References

- Abazajian, K., Adelman-McCarthy, J. K., Agüeros, M. A., et al. 2004, *AJ*, 128, 502
- Abdurro'uf, Accetta, K., Aerts, C., et al. 2022, *ApJS*, 259, 35
- Abomalima, A. & Frebel, A. 2018, *ApJS*, 238, 36
- Aguado, D. S., Youakim, K., González Hernández, J. I., et al. 2019, *MNRAS*, 490, 2241
- Aihara, H., Allende Prieto, C., An, D., et al. 2011, *ApJS*, 193, 29
- Allende Prieto, C. 2023, *Atoms*, 11, 61
- Allende Prieto, C., Beers, T. C., Wilhelm, R., et al. 2006, *ApJ*, 636, 804
- Allende Prieto, C., Koesterke, L., Hubeny, I., et al. 2018, *A&A*, 618, A25
- An, D., Beers, T. C., & Chiti, A. 2024, arXiv e-prints, arXiv:2404.14626
- Andrae, R., Fouesneau, M., Sordo, R., et al. 2023a, *A&A*, 674, A27
- Andrae, R., Rix, H.-W., & Chandra, V. 2023b, *ApJS*, 267, 8
- Aoki, W., Li, H., Matsuno, T., et al. 2022, *ApJ*, 931, 146
- Aoki, W., Tominaga, N., Beers, T. C., Honda, S., & Lee, Y. S. 2014, *Science*, 345, 912
- Avdeeva, A. S., Kovaleva, D. A., Malkov, O. Y., & Zhao, G. 2024, *MNRAS*, 527, 7382
- Bellazzini, M., Massari, D., De Angeli, F., et al. 2023, *A&A*, 674, A194
- Belokurov, V. & Kravtsov, A. 2022, *MNRAS*, 514, 689
- Binney, J. & Vasiliev, E. 2024, *MNRAS*, 527, 1915
- Bohlin, R. C., Deustua, S. E., & de Rosa, G. 2019, *AJ*, 158, 211
- Bohlin, R. C., Gordon, K. D., & Tremblay, P. E. 2014, *PASP*, 126, 711
- Bohlin, R. C. & Lockwood, S. 2022, Update of the STIS CTI Correction Formula for Stellar Spectra, Instrument Science Report STIS 2022-7, 11 pages
- Buder, S., Sharma, S., Kos, J., et al. 2021, *MNRAS*, 506, 150
- Cardelli, J. A., Clayton, G. C., & Mathis, J. S. 1989, *ApJ*, 345, 245
- Carrasco, J. M., Weiler, M., Jordi, C., et al. 2021, *A&A*, 652, A86
- Castelli, F., Gratton, R. G., & Kurucz, R. L. 1997, *A&A*, 318, 841
- Chandra, V., Semenov, V. A., Rix, H.-W., et al. 2023, arXiv e-prints, arXiv:2310.13050
- Chen, B., Hayden, M. R., Sharma, S., et al. 2023, *MNRAS*, 523, 3791
- Chiti, A., Frebel, A., Mardini, M. K., et al. 2021, *ApJS*, 254, 31
- Coelho, P., Barbuy, B., Meléndez, J., Schiavon, R. P., & Castilho, B. V. 2005, *A&A*, 443, 735
- Conroy, C., Weinberg, D. H., Naidu, R. P., et al. 2022, arXiv e-prints, arXiv:2204.02989
- Cooper, A. P., Koposov, S. E., Allende Prieto, C., et al. 2023, *ApJ*, 947, 37
- Cropper, M., Katz, D., Sartoretti, P., et al. 2018, *A&A*, 616, A5
- Cui, X.-Q., Zhao, Y.-H., Chu, Y.-Q., et al. 2012, *Research in Astronomy and Astrophysics*, 12, 1197
- De Angeli, F., Weiler, M., Montegriffo, P., et al. 2023, *A&A*, 674, A2
- de Jong, R. S., Agertz, O., Berbel, A. A., et al. 2019, *The Messenger*, 175, 3
- de Silva, G. M., Freeman, K. C., Bland-Hawthorn, J., et al. 2015, *MNRAS*, 449, 2604
- Deason, A. J. & Belokurov, V. 2024, arXiv e-prints, arXiv:2402.12443
- Fallos, C. P. & Sanders, J. L. 2024, arXiv e-prints, arXiv:2405.10699
- Gaia Collaboration, Brown, A. G. A., Vallenari, A., et al. 2016, *A&A*, 595, A2
- Gaia Collaboration, Montegriffo, P., Bellazzini, M., et al. 2023a, *A&A*, 674, A33
- Gaia Collaboration, Vallenari, A., Brown, A. G. A., et al. 2023b, *A&A*, 674, A1
- García Pérez, A. E., Allende Prieto, C., Holtzman, J. A., et al. 2016, *AJ*, 151, 144
- Green, G. M. 2018, *The Journal of Open Source Software*, 3, 695
- Gregg, M. D., Silva, D., Rayner, J., et al. 2006, in *The 2005 HST Calibration Workshop: Hubble After the Transition to Two-Gyro Mode*, ed. A. M. Koekoemoer, P. Goudfrooij, & L. L. Dressel, 209
- Gustafsson, B., Edvardsson, B., Eriksson, K., et al. 2008, *A&A*, 486, 951
- Hattori, K. 2024, arXiv e-prints, arXiv:2404.01269
- Heger, A. & Woosley, S. E. 2010, *ApJ*, 724, 341
- Huang, B., Yuan, H., Xiang, M., et al. 2024, *ApJS*, 271, 13
- Husser, T. O., Wende-von Berg, S., Dreizler, S., et al. 2013, *A&A*, 553, A6
- Imig, J., Price, C., Holtzman, J. A., et al. 2023, *ApJ*, 954, 124
- Jin, S., Trager, S. C., Dalton, G. B., et al. 2024, *MNRAS*, 530, 2688
- Klessen, R. S. & Glover, S. C. O. 2023, *ARA&A*, 61, 65
- Kollmeier, J. A., Zasowski, G., Rix, H.-W., et al. 2017, arXiv e-prints, arXiv:1711.03234
- Komiya, Y., Habe, A., Suda, T., & Fujimoto, M. Y. 2010, *ApJ*, 717, 542
- Koutsouridou, I., Salvadori, S., Skúladóttir, Á., et al. 2023, *MNRAS*, 525, 190
- Laroche, A. & Speagle, J. S. 2024, arXiv e-prints, arXiv:2404.07316
- Lejeune, T., Cuisinier, F., & Buser, R. 1998, *A&AS*, 130, 65
- Leung, H. W. & Bovy, J. 2019, *MNRAS*, 483, 3255
- Leung, H. W. & Bovy, J. 2024, *MNRAS*, 527, 1494
- Li, H., Aoki, W., Matsuno, T., et al. 2022a, *ApJ*, 931, 147

- Li, J., Wong, K. W. K., Hogg, D. W., Rix, H.-W., & Chandra, V. 2023, arXiv e-prints, arXiv:2309.14294
- Li, X. & Lin, B. 2023, MNRAS, 521, 6354
- Li, Z., Zhao, G., Chen, Y., Liang, X., & Zhao, J. 2022b, MNRAS, 517, 4875
- Lian, J., Zasowski, G., Mackereth, T., et al. 2022, MNRAS, 513, 4130
- Luo, A. L., Zhang, H.-T., Zhao, Y.-H., et al. 2012, *Research in Astronomy and Astrophysics*, 12, 1243
- Majewski, S. R., Schiavon, R. P., Frinchaboy, P. M., et al. 2017, *AJ*, 154, 94
- Mardini, M. K., Frebel, A., & Chiti, A. 2024, MNRAS, 529, L60
- Martin, N. F., Starkenburg, E., Yuan, Z., et al. 2023, arXiv e-prints, arXiv:2308.01344
- Montegriffo, P., De Angeli, F., Andrae, R., et al. 2023, A&A, 674, A3
- Naidu, R. P., Conroy, C., Bonaca, A., et al. 2020, *ApJ*, 901, 48
- Ness, M., Hogg, D. W., Rix, H. W., Ho, A. Y. Q., & Zasowski, G. 2015, *ApJ*, 808, 16
- Nomoto, K., Kobayashi, C., & Tominaga, N. 2013, *ARA&A*, 51, 457
- Nomoto, K., Tominaga, N., Umeda, H., Kobayashi, C., & Maeda, K. 2006, *Nucl. Phys. A*, 777, 424
- Onken, C. A., Wolf, C., Bessell, M. S., et al. 2024, arXiv e-prints, arXiv:2402.02015
- Pal, T., Khan, I., Worthey, G., Gregg, M. D., & Silva, D. R. 2023, *ApJS*, 266, 41
- Paszke, A., Gross, S., Chintala, S., et al. 2017, in *NIPS 2017 Workshop on Autodiff*
- Paszke, A., Gross, S., Massa, F., et al. 2019, in *Advances in Neural Information Processing Systems*, ed. H. Wallach, H. Larochelle, A. Beygelzimer, F. d'Alché-Buc, E. Fox, & R. Garnett, Vol. 32 (Curran Associates, Inc.)
- Powell, M. J. D. 2002, *Mathematical Programming*, 92, 555
- Rix, H.-W., Chandra, V., Andrae, R., et al. 2022, *ApJ*, 941, 45
- Salvadori, S., Schneider, R., & Ferrara, A. 2007, MNRAS, 381, 647
- Sanders, J. L. & Matsunaga, N. 2023, MNRAS, 521, 2745
- Sarmiento, R., Scannapieco, E., & Côté, B. 2019, *ApJ*, 871, 206
- Sartoretti, P., Katz, D., Cropper, M., et al. 2018, A&A, 616, A6
- Schlafly, E. F. & Finkbeiner, D. P. 2011, *ApJ*, 737, 103
- Schlegel, D. J., Finkbeiner, D. P., & Davis, M. 1998, *ApJ*, 500, 525
- Schönrich, R. & Binney, J. 2009, MNRAS, 399, 1145
- Sharma, S., Hayden, M. R., & Bland-Hawthorn, J. 2021, MNRAS, 507, 5882
- Tarumi, Y., Hartwig, T., & Magg, M. 2020, *ApJ*, 897, 58
- Taylor, M. B. 2005, in *Astronomical Society of the Pacific Conference Series*, Vol. 347, *Astronomical Data Analysis Software and Systems XIV*, ed. P. Shopbell, M. Britton, & R. Ebert, 29
- Ting, Y.-S., Conroy, C., Rix, H.-W., & Cargile, P. 2019, *ApJ*, 879, 69
- Ting, Y.-S., Rix, H.-W., Conroy, C., Ho, A. Y. Q., & Lin, J. 2017, *ApJ*, 849, L9
- Weiler, M., Carrasco, J. M., Fabricius, C., & Jordi, C. 2023, A&A, 671, A52
- Wilson, J. C., Hearty, F. R., Skrutskie, M. F., et al. 2019, *PASP*, 131, 055001
- Witten, C. E. C., Aguado, D. S., Sanders, J. L., et al. 2022, MNRAS, 516, 3254
- Xiang, M., Rix, H.-W., Ting, Y.-S., et al. 2022, A&A, 662, A66
- Xiang, M., Ting, Y.-S., Rix, H.-W., et al. 2019, *ApJS*, 245, 34
- Xiao, K., Yuan, H., Huang, B., et al. 2023a, *ApJS*, 268, 53
- Xiao, K., Yuan, H., López-Sanjuan, C., et al. 2023b, *ApJS*, 269, 58
- Xylakis-Dornbusch, T., Christlieb, N., Hansen, T. T., et al. 2024, arXiv e-prints, arXiv:2403.08454
- Yamada, S., Suda, T., Komiyama, Y., Aoki, W., & Fujimoto, M. Y. 2013, MNRAS, 436, 1362
- Yan, H., Li, H., Wang, S., et al. 2022, *The Innovation*, 3, 100224
- Yao, Y., Ji, A. P., Kopusov, S. E., & Limberg, G. 2024, MNRAS, 527, 10937
- York, D. G., Adelman, J., Anderson, John E., J., et al. 2000, *AJ*, 120, 1579
- Youakim, K., Starkenburg, E., Martin, N. F., et al. 2020, MNRAS, 492, 4986
- Zhang, X., Green, G. M., & Rix, H.-W. 2023, MNRAS, 524, 1855
- Zhao, G., Chen, Y.-Q., Shi, J.-R., et al. 2006, *Chinese J. Astron. Astrophys.*, 6, 265
- Zhao, G., Zhao, Y.-H., Chu, Y.-Q., Jing, Y.-P., & Deng, L.-C. 2012, *Research in Astronomy and Astrophysics*, 12, 723